Collisional cooling of internal rotation in MgH^+ ions trapped with He atoms: Quantum modeling meets experiments in Coulomb crystals

L. González-Sánchez,[1] R. Wester,[2] and F. A. Gianturco[2,*]

[1]*Departamento de Química Física, University of Salamanca, Plaza de los Caídos sn, 37008 Salamanca, Spain*

[2]*Institut für Ionenphysik und Angewandte Physik, Universitaet Innsbruck, Technikerstr. 25, A-6020, Innsbruck, Austria*

(Received 8 July 2018; published 15 November 2018)

Using the *ab initio* computed potential energy surface for the electronic interaction of the $MgH^+(^1\Sigma)$ ion with the $He(^1S)$ atom, we calculate the relevant state-changing rotationally inelastic collision cross sections from a quantum treatment of the multichannel scattering problem. We focus on the quantum dynamics at the translationally low energies for the present partners discussed in earlier, cold ion trap experiments (see below), which we wish to model in detail. The corresponding state-changing rates computed between the lower rotational states of the molecular ion are employed to describe the time-evolution kinetics followed by recent experiments on Coulomb-crystallized $MgH^+(^1\Sigma)$, where the ions are rotationally cooled by micromotion tuning after being uploaded into the trap of He as a buffer gas. The present computational modeling of the final ion rotational temperatures in the experiments turns out to agree very well with the observations and points at a fast equilibration between rotational and thermal temperatures of the ions.

DOI: 10.1103/PhysRevA.98.053423

I. INTRODUCTION

Detailed control (for a general overview see [1]) and active manipulation of the internal, as well as the external, degrees of freedom of gas-phase molecules have been pursued and investigated for the best part of the last 20 years [2–4] and the information obtained has been of great value for furthering advances in several experimental fields. Hence, from the progress in methodology [5], to quantum information processing [6], to quantum control of molecular reactions and transformations [7], and to collection of accurate data for chemical reactions in well-defined states [8], a great number of studies and of computational models have been developed. They have involved a large variety of ensembles of cold molecules which could be further experimentally investigated to follow their time evolutions from well-defined initial conditions and to extract specific information on their state-to-state collision rate constants [9].

From these many fields of investigation research on the behavior of cold molecules, whether neutral or ionic species, has developed fairly rapidly via the use of a wide variety of techniques which are not further discussed in this study, as they have been presented various times in the current literature [10–16].

Cooling techniques for molecular ions have also developed to the point where it has become realistically possible to work with ensembles of molecular ions that are sympathetically cooled into Coulomb crystallization through an efficient Coulomb interaction with laser-cooled atomic ions [15]. The above techniques have shown that translational-cooling schemes are indeed very versatile in bringing the molecular ions down to low, millikelvin temperatures [15], although further passage to also achieve simultaneously extremely low-lying internal states' being the most populated in the cold traps has to be designed and adapted to the specific molecules under study [15].

In very recent analyses [17,18], a setting has been experimentally investigated wherein the usual helium buffer-gas technique for the cooling of internal molecular degrees of freedom has been employed for $MgH^+(^1\Sigma)$ ions. The ions were previously trapped in a cryogenically cooled, linear, radio-frequency quadrupole trap and further translationally cooled, through a Coulomb-type interaction, with simultaneously trapped, laser-cooled atomic Mg^+ ions [17]. It was found there that the interaction with the additional He buffer gas is chiefly employed for cooling of the molecular ion's internal degrees of freedom, thereby requiring much lower gas densities (e.g., around 10^{10} cm^{-3}) for the uploaded buffer atoms, which can therefore be four to five orders of magnitude lower than in a typical buffer-gas cooling setting [18]. The vibrational degree of freedom of the MgH^+ partner is known to be already frozen out at room temperature, with $>99\%$ probability that the molecular ion will be in its vibrational ground state. Hence, at the cryogenic temperatures of Coulomb crystallization it can be entirely disregarded when modeling the present dynamics, so that the full rotational-state distributions of the cold molecules can be directly measured in the Coulomb trap [17].

In the present work we analyze in detail this specific collisional cooling process, which involves the differently populated rotational states of MgH^+ when the He atoms of the buffer gas are uploaded into the trap after the formation of Coulomb-crystallized ions.

The following section (II) provides specific information on the potential energy surface (PES) we have computed for the MgH^+ plus He system and further outlines the quantum dynamics of the rotationally inelastic collision processes. Sec-

*Corresponding author: francesco.gianturco@uibk.ac.at

tion III analyzes the relevant state-changing cross sections and Sec. IV uses them to generate the state-changing rates at the temperature of the traps. The master equations describing the system's time evolution as a function of various trap parameters plus conditions are presented and discussed in Sec. V. The final section, VI, summarizes our present conclusions.

II. INTERACTION FORCES AND QUANTUM DYNAMICS

Within the usual Born-Oppenheimer approximation that separates nuclear and electronic motions, the electronic interaction between the $MgH^+(^1\Sigma)$ molecular ion at its equilibrium geometry of 1.67 Å and the $He(^1S)$ neutral atom is described by a two-dimensional (2D) grid of points providing the $V(R,\theta)$ single PES. In our earlier work on the same system [19,20], we computed the points using the coupled-cluster (CC) single and double excitations with noniterative corrections for the triple excitation and initial expansion coupled with a complete basis set extrapolation limit and starting with the augmented coupled-cluster polarized valence multipole (auf-cc-pVnZ) (with $n = 3, 4, 5$) basis set series as implemented in the software package GAUSSIAN08 [21]. The employed Jacobi coordinates were the distance R of the He atom from the center of mass of MgH^+ and the angle θ between R and the bond, r_{eq}, of the partner molecular ion. The angular values were varied between 0 and 180 in intervals of 10. The radial coordinate ranged from 1.7 to 16.0 Å, generating a total of 1200 radial points for the full set of angles mentioned before. In the current work we have taken advantage of the previous set of computed points on the 2D grid but we have added several new points to better describe the short-range repulsive interaction over a broad range of angles. Thus, an additional set of 100 points was added to the previous 2D grid.

The marked anisotropy of the present PES has been extensively discussed [19,20] so we do not repeat the same analysis here. Suffice it to say that the most attractive well of the overall interaction is located along a linear structure, with the He atom approaching the Mg^+ side of the molecular partner. The same PES becomes increasingly more repulsive as the He atom approaches the partner from the H-atom end of the molecular cation. Thus, the multipolar representation of the anisotropic interaction can be obtained by writing

$$V(R,\theta|r_{eq}) = \sum_{\lambda}^{\lambda_{max}} V_\lambda(R|r_{eq}) P_\lambda(\cos\theta), \tag{1}$$

where

$$V_\lambda(R|r_{eq}) = \int_{-1}^{1} V(R,\theta|r_{eq}) P_\lambda(\cos\theta)\, d\cos\theta. \tag{2}$$

Hence, the range of action of each V_λ coefficient gives us an indication of the strength and range of the anisotropy present in the computed PES: each coefficient, in fact, will be directly involved in the dynamical coupling of rotational states of the cation during the collisional inelastic processes within the Coulomb trap, as we discuss below. We have reached good numerical convergence of expansion (1) by extending the sum up to $\lambda_{max} = 30$. As an example of the radial behavior of the coefficients from Eq. (2), we report in Fig. 1 the first six

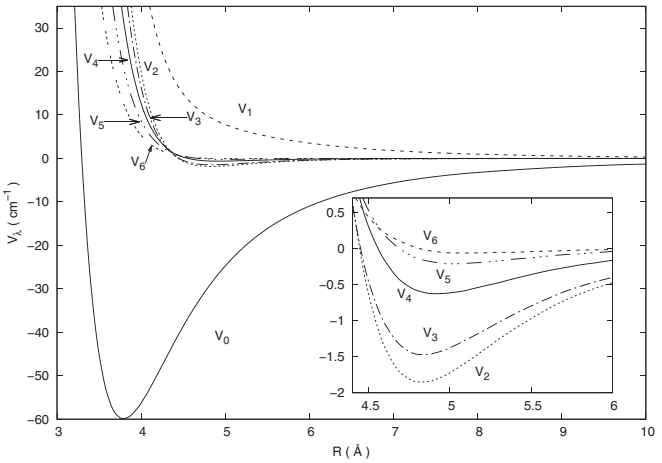

FIG. 1. Computed multipolar coefficients from Eq. (2) for the MgH^+ plus He system. Only the first six coefficients are reported here.

coefficients for the present PES. The inset in this figure shows an enlarged view of the higher multipolar terms, beyond $\lambda = 0$ and 1, in the radial regions where the coefficients with λ values of 2, 3, 4, and 5 present an attractive behavior, albeit with decreasing depth as the λ value increases, while the next-higher term shows a much shallower well. All these terms, however, are markedly less attractive than the dominant spherical term with $\lambda = 0$ shown in the figure.

Since the data in Fig. 1 mainly describe the short-range and the inner well regions, we need to further include the long-range (LR) behavior of the total PES. This is done by a numerical interpolation between short-range and LR regions included in our in-house scattering code (see below) and it turns out to show as its strongest attractive term the LR spherical polarizability contribution which appears in the standard treatment of the LR forces via perturbative expansions (e.g., see [22]):

$$V(R,\theta|r_{eq}) \overset{R\to\infty}{=} V_{LR}(R,\theta) \sim -\frac{\alpha_{He}}{2R^4} - 2\alpha_{He}\frac{\mu P_1(\cos\theta)}{R^5} - \frac{\alpha_{He}\mu^2}{R^6} \tag{3}$$

$$- (\alpha_{He}\mu^2 + Q\alpha_{He})\frac{P_2(\cos\theta)}{R^7} \tag{4}$$

$$+ \ldots. \tag{5}$$

The above array of asymptotic terms is dominated by the spherical term in the $\lambda = 0$ coefficient. On the other hand, the coefficients with $\lambda = 1$ and $\lambda = 2$ are next in importance with respect to the next-higher coefficients, as one could also gather from the relative strengths of their short-range terms shown in Fig. 1. Hence, we can qualitatively say that the rotational inelasticity at low collision energies will be mainly driven by the $\Delta j = 1$ and $\Delta j = 2$ rotational coupling terms of the PES, as we discuss further below.

Once the full PES has been obtained and its multipolar coefficients generated from Eqs. (1)–(3), including the coefficients for the LR extension of the lowest three λ values, one can approach the calculations for the quantum multichannel

dynamics of the inelastic scattering processes inducing state changes between rotational levels of the cation, taken to be in its $|v \geqslant 0$ vibrational state: we therefore describe the nuclear motion of the partners within the usual time-independent Schrödinger equation containing the potential interaction of Eq. (1) and subjected to the usual boundary conditions within the coupled-channel approach of expanding the total wave functions on an ensemble of rotational functions for the molecular ion plus the continuum functions for the relative motion, numerically obtained at the positive, relative collision energies of the scattering partners [23].

We have employed our in-house numerical code ASPIN and details of its implementation have been given before [24,25]. We therefore do not discuss it again in the present work. Suffice it to say that the physical observables which we obtain from the ASPIN scattering code are in this case the state-to-state partial cross sections for each of the contributing total angular momenta J: $\sigma^J(j' \leftarrow j|E_i)$, with E_i giving the initial relative energy between partners. The further summation over the contributing angular momenta (which, in the present case, was taken up to $J_{\max} = 50$) will therefore yield the corresponding state-to-state partial integral cross sections:

$$\sigma(j' \leftarrow j|E_i) = \sum_{J}^{J_{\max}} \sigma^J(j' \leftarrow j|E_i). \tag{6}$$

From them we can further obtain the partial rotational quenching and heating rate constants $K_{jj'}(T)$ at the temperature of interest:

$$K_{jj'}(T) = \int \sigma(j' \leftarrow j|E) \sqrt{\frac{4E}{\pi(k_B T)^3}} \exp(-E/k_B T) E dE. \tag{7}$$

We have integrated the computed cross sections over an extended range of collision energies for the corresponding cross sections, ensuring that the threshold behavior is well described by a dense grid of values. We have further used and extended the range of energies well beyond the extension necessary to map the required interval of temperatures. Numerical convergence has been checked to more than 0.01 stability of the final rates.

III. COMPUTING THE STATE-CHANGING COLLISION CROSS SECTIONS

As mentioned earlier, the inelastic cross sections were obtained using our in-house quantum CC code ASPIN [25–27]. Therefore, we report here only a few specific details of the numerical procedure. We have included in each CC calculation a maximum number of rotational channels up to $j_{\max} = 11$, where at each collision energy at least five channels were included as closed channels, to ensure overall convergence of the inelastic cross sections.

The radial integration was extended, at the lowest collision energies which we needed to take into consideration, out to $R_{\max} = 1000$ Å. The anisotropy of the PES was also included via a variable number of λ values in the expansions of Eqs. (1) and (2). In practice, we found that we obtained converged inelastic cross sections by keeping $\lambda_{\max} = 18$ in our potential

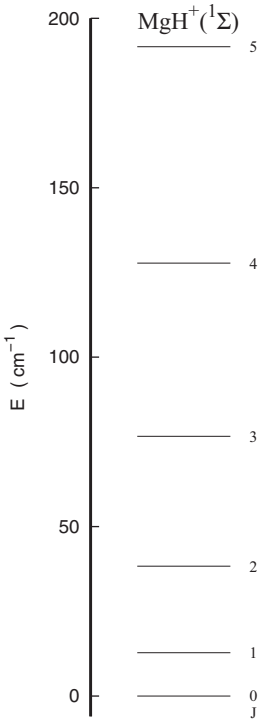

FIG. 2. Computed rotational energy spacings between the lower five molecular levels of the ion which are included in the present dynamical analysis of the collisional rotational energy transfer.

expansion. The B_0 value for the MgH^+ rotor was taken to be 6.3870 cm^{-1} [28,29]. It is worth noting here that the present calculations cover a range of energies and temperatures which is much higher than that studied earlier by us on the present system [19,20]. This therefore means that all the present cross sections were not among those discussed in that earlier work.

The data in Fig. 2 show a pictorial presentation of the energy spacing for the lower rotational states of the MgH^+ cation considered in the present study. One clearly sees in the figure how the lower three rotational levels are the closest in energy and will be the ones more effectively activated at the collisional temperatures of the present study. To reach numerical convergence of the state-changing cross sections from Eq. (6), however, we have included in the CC state expansion also the higher rotational levels shown in Fig. 2.

The significant role played by anisotropic features of the PES, in conjunction with the values of the energy gaps between transitions, is shown by the partial excitation cross sections reported in Fig. 3. The upper panel shows excitation processes with $\Delta j > 1$ transitions, while the processes involving $\Delta j = 1$ transitions are shown in the lower panel.

The marked interaction forces which act during collisional events cause a very rich presence of resonant features, especially above the onset energies of the excitation precesses and for transitions involving the lower rotational states. Such marked structural features are obviously linked to the occurrence of both open-channel (trapping) resonances and virtual excitations via Feshbach resonances involving closed rotational channels. A detailed analysis of the dynamical origins of such resonances is not carried out here, as it is

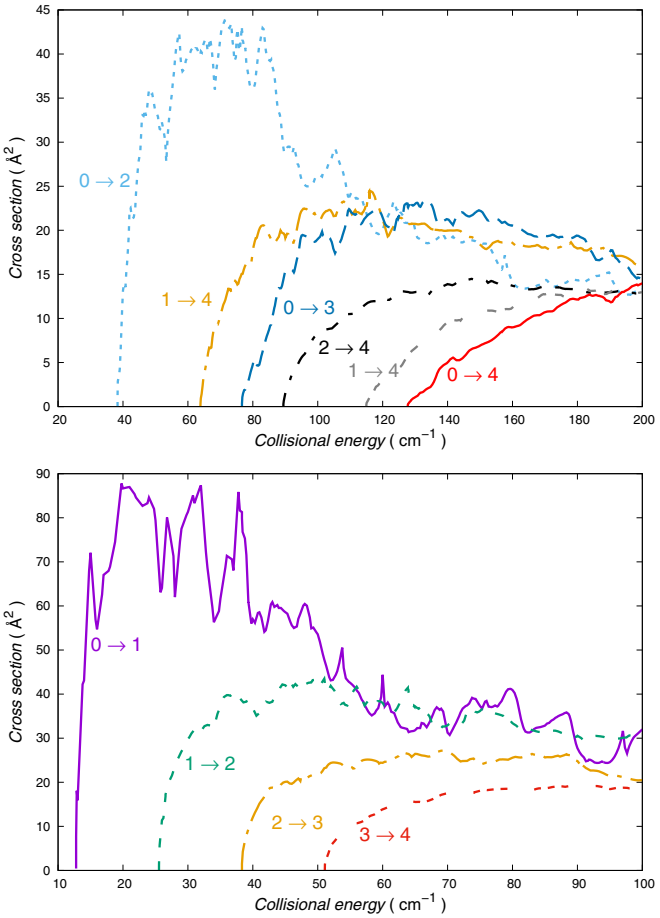

FIG. 3. Computed excitation cross sections for collisional state-changing processes in the cold trap. The examined range of relative energies spans 100 cm^{-1}. Upper panel: Excitation processes for $\Delta j > 1$. Lower panel: Excitation collisions for $\Delta j = 1$ transitions.

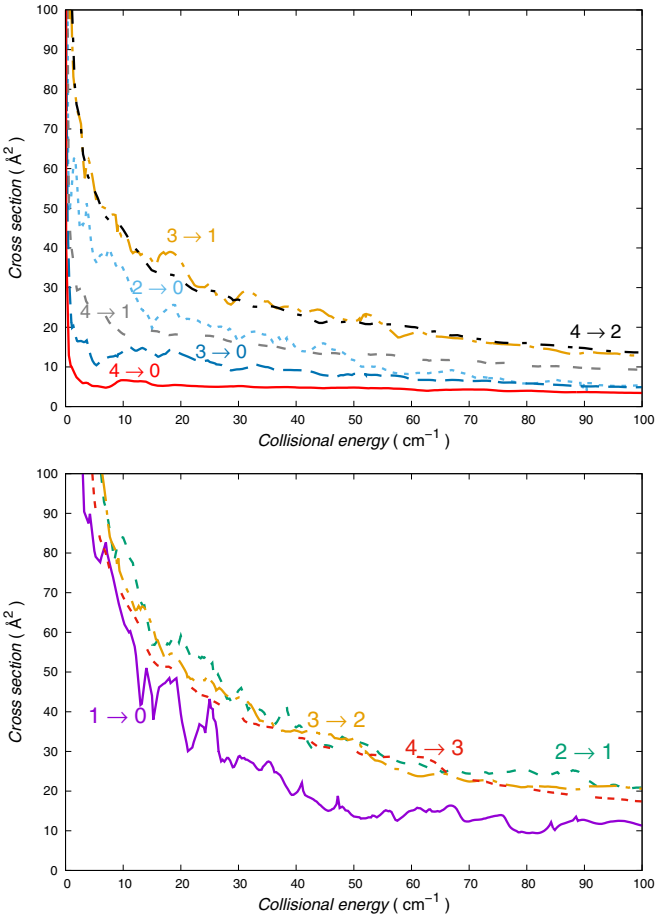

FIG. 4. Computed rotationally inelastic cross sections associated with the de-excitation paths from the lower rotational states of the molecular ion. Upper panel: Rotational de-excitation processes with $\Delta j > 1$. Lower panel: Rotational "cooling" processes for $\Delta j = 1$ transitions. See the text for further details.

somewhat outside the scope of the present study. However, it is interesting to point out that near each threshold the two dominant excitation processes are those where the ground rotational state of the target ion is excited via the $\Delta j = 1$ coupling potential and the $\Delta j = 2$ dynamical potential term. As discussed earlier regarding the PES features in Fig. 1, the largest cross sections pertain to the effects of anisotropic coupling linked to the $\lambda = 1$ multipolar coefficient and to the extension of its radial range during the dynamics. On the other hand, the next cross section in size is that for which it is the $\lambda = 2$ potential coupling which chiefly causes the $(0 \rightarrow 2)$ rotational excitation process shown in the upper panel in Fig. 3. On the whole, however, the data for the excitation processes show the state-changing dynamics to be an effective collisional path for the target ion at the low collision energies shown here.

The data reported in Fig. 4 present the corresponding inelastic transitions relevant for the collisional rotational "cooling" (i.e., rotational de-excitation) dynamics in the trap. These de-excitation cross sections indicate that the relative sizes of the inelastic transitions with $\Delta j = -1$ (lower panel in Fig. 4) decrease as the initial state moves up the energy ladder. This signifies that the processes where more internal rotational energy is released into the trap after the collision are more efficient since the interaction times are shorter in comparison to the case where the least energy is being released [e.g., for the $(1 \rightarrow 0)$ process] and the de-excitation dynamics is least effective. On the other hand, when the rotational internal energy released becomes even higher (upper panel in Fig. 4), the presence of $\Delta j > 1$ couplings makes the dynamical torques activated by the higher terms of the multipolar potential of Eq. (1) less efficient so that all these inelastic cross sections are uniformly smaller than those with $\Delta j = 1$ state-changing processes. Here again, however, we see that the cross sections are rather significant in size and indicate the inelastic collisions to be an effective path for depopulating the rotational states of the trapped molecular ions.

IV. ROTATIONALLY INELASTIC RATES AT LOW T ($\leqslant$50 K)

Following the relation shown by Eq. (7) we have employed the inelastic cross sections discussed in the previous section to obtain the corresponding inelastic rates over a broad range of temperatures, spanning those of the Coulomb-crystal experiments [16].

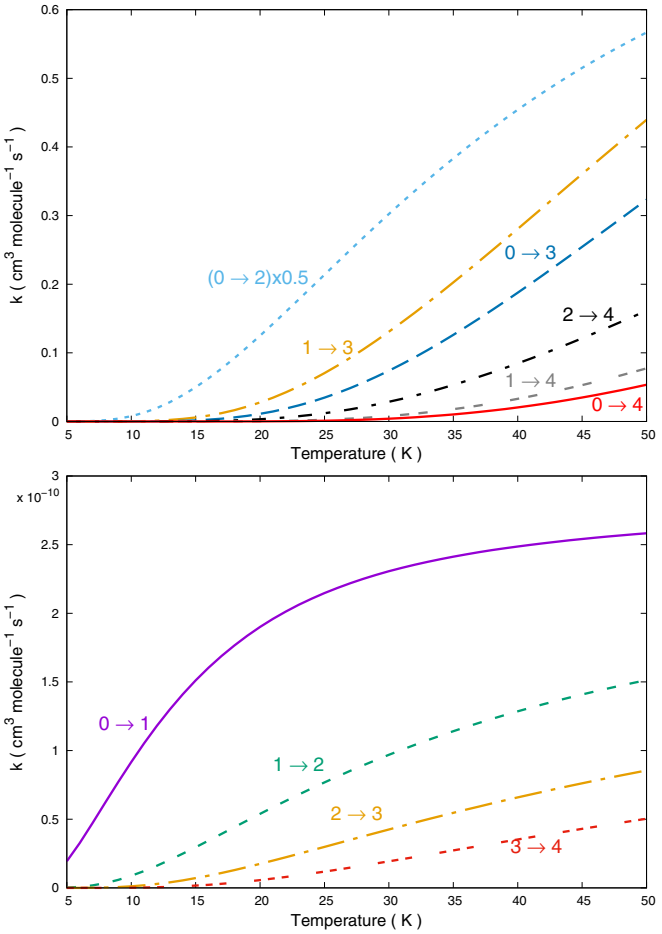

FIG. 5. Computed rotational 'heating' (excitation) rates between different rotational states of MgH^+ in the traps. Upper panel: Excitation rates with $\Delta j > 1$. Lower panel: Excitation rates for $\Delta j = 1$ transitions. See the text for further details.

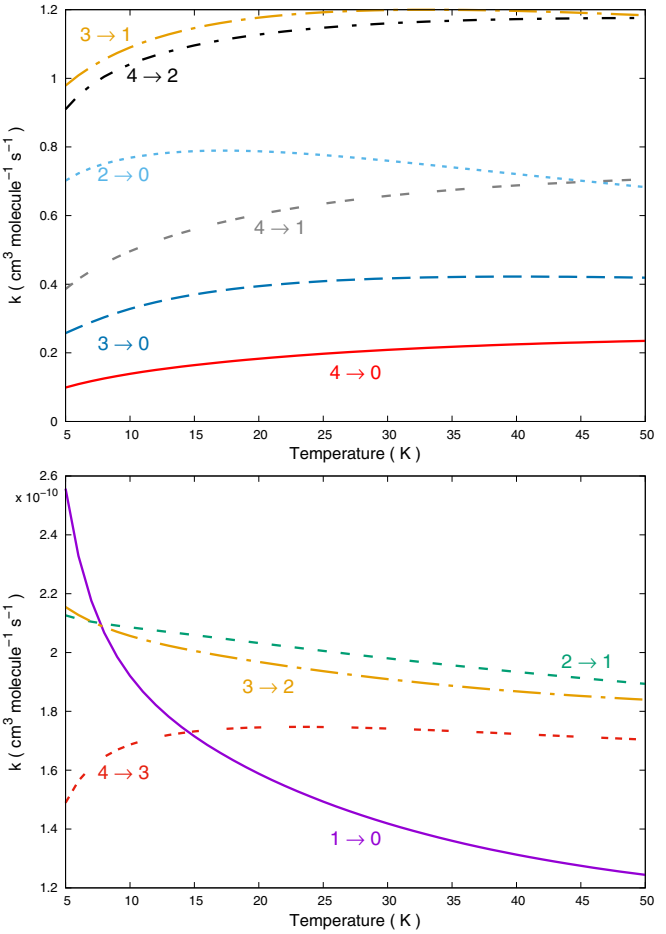

FIG. 6. Same as Fig. 5, but this time for the 'cooling' (de-excitation) rates between rotational states. Upper panel: Inelastic rates with a negative $\Delta j > -1$. Lower panel: Transitions with a negative $\Delta j = -1$. See the text for further details.

The data in Figs. 5 and 6 present the state-to-state inelastic rates involving the lower five rotational states of the MgH^+ trapped ion. More specifically, the excitation rates reported in the upper panel in Fig. 5 show the processes for which the state-changing transitions involve $\Delta j > 1$ transitions, while the lower panel presents the transition rates with $\Delta j = 1$ and involving rotational states from $|0\rangle$ up to $|4\rangle$. The following considerations were made upon examining the results given in the figure:

(1) The cooling rates rapidly become fairly high as the collision energy increases and show the $(0 \rightarrow 1)$ excitation to be by far the largest. All other single-quantum excitations from higher states of the ion show rates which are lower than the $(0 \rightarrow 1)$ rate by a factor of 2 or more.

(2) The multiquantum excitation rates are seen to be somewhat lower than the former ones (see upper panel in Fig. 5) and remain nearly one order of magnitude lower in the temperature regions between 10 and 30 K.

(3) In both sets of processes the excitation from the ground rotational state corresponds to the highest values of the excitation rates in each panel.

It is interesting to note that in a recent study of ours on a similar molecular cation, the $OH^+(^2\Sigma)$ molecule [29], the rotational excitation rates computed in a trap with He as a buffer gas turned out to be about a factor of 3 lower over the same range of temperatures, in keeping with differences between the energy spacings of their lower-lying rotational levels.

If we now turn to the rotational relaxation rates over the same range of temperatures, we see in Fig. 6 their relative size and T dependence. The lower panel reports single-quantum rotational "cooling" transitions, while multiple-quantum rotational de-excitation transitions are shown in the upper panel.

The general trend of the relative sizes of the inelastic rotational de-excitation transitions is here very similar to that of the excitation rates. However, with the exception of the $(1 \rightarrow 0)$ process, all the computed rates show a fairly slow dependence on the temperature, a result which is in keeping with the same findings from our earlier calculations regarding the OH^+ and/or He system [29]. The single-quantum rotational relaxation rates are also uniformly higher than those for two- and three-quantum transitions, which are in some cases up to one order of magnitude lower. The same size differences were also found for the $OH^+(^2\Sigma)$ cation [29].

V. MODELING THE COOLING KINETICS IN THE TRAP

As discussed in Sec. I, the experimental findings in Ref. [18] indicate that the He buffer gas uploaded within the setting of MgH^+ ions trapped in a cryogenically cooled linear, radio-frequency quadrupole trap, and already translationally cooled through Coulomb interaction with atomic Mg^+ ions, can cause the molecular ions to be cooled into their ground rotational state even though a low density of He atoms, $\sim 10^{10}$ cm^{-3}, is present in the trap. In those experiments, in fact, the He temperature is essentially kept constant while the effective collision "temperature" is changed via scaling of the average micromotion amplitude. In this way, the molecular ions experience different effective temperatures within the uploaded gas environment (see Ref. [18] for further details).

Given the information we have obtained from the calculations presented in the previous sections, we are now in a position to try and follow the microscopic evolutions of the cation's rotational-state populations by setting up the corresponding rate equations describing such evolution as induced by collisional energy transfer with the uploaded He atoms in the trap [30,31],

$$\frac{d\mathbf{p}}{dt} = n_{\mathrm{He}}\mathbf{k}(T)\cdot\mathbf{p}(t), \tag{8}$$

where the quantity n_{He} indicates the density of He atoms in the trap, the vector $\mathbf{p}(t)$ contains the time-evolving fractional rotational populations of the ion partner's rotational state, $p_j(t)$, from the initial conditions at $t = t_{\mathrm{initial}}$, and the matrix $\mathbf{k}(T)$ contains the individual $k_{i\to j}(T)$ rate coefficients at the temperature of the trap's conditions. Both the $p(t_{\mathrm{initial}})$ values and the collisional temperature T of the trap corresponding to the mean collisional energy between the partners are quantities to be specifically selected in each computational run and are discussed in detail in the modeling examples presented below. In the present study we disregard for the moment the inclusion of the state-changing rates due to spontaneous radiative processes in the trap. These quantities are already known to be smaller than the collisionally controlled rates between the lower rotational levels of such systems, as shown by us in earlier studies [31], and are therefore not expected to have a significant effect under the present trap conditions [18].

We have chosen the initial rotational temperature of the trap's ions to be at 400 K, so that the vector's components at $t = t_{\mathrm{initial}}$ are given by a Boltzmann distribution at that chosen temperature. This was done in order to follow the kinetics evolution over an extended range of time and also test the physical reliability of our computed state-changing collisional rates. Obviously the actual kinetics evolution of physical interest in this study is considered over the range of the much lower temperatures sampled in the experiments [18].

If the rate coefficients of the $\mathbf{K}(T)$ matrix satisfy the detailed balance between state-changing transitions, then as $t \to \infty$ the initial Boltzmann distribution will approach that of the effective equilibrium temperature of the uploaded buffer gas as felt by the ions in the Coulomb crystals. These asymptotic solutions correspond to the steady-state conditions in the trap and can be obtained by solving the corresponding homogeneous form of Eq. (8), given as $d\mathbf{p}(t)/dt = 0$. We solved the homogeneous equations by using the singular-value decomposition technique [30], employed by us in previous studies. The nonhomogeneous Eqs. (8), starting from our t_{initial} of 400 K, were solved using the Runge-Kutta method for different translational temperatures of the trap. Since the role of the He density is simply that of a scaling factor in the kinetics equations, we present in the figures only the actual value which was employed in the trap experiments [18].

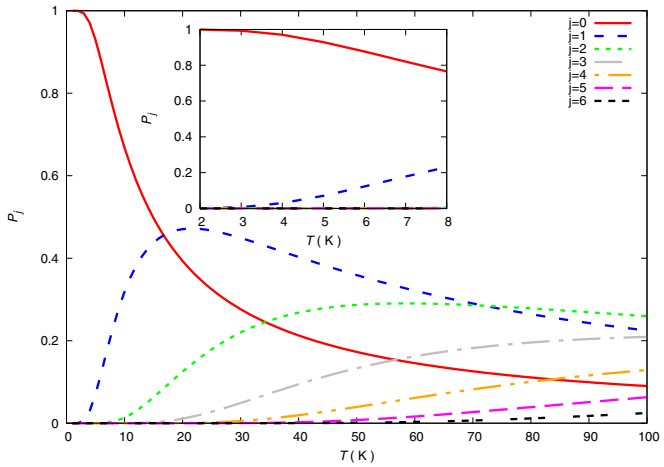

FIG. 7. Asymptotic (steady-state) rotational populations of the MgH^+ internal states as a function of the computed trap translational temperatures up to 100 K. Inset: Data for the lower T values, up to $\sim$8 K. See the text for further details.

The results shown in Fig. 7 indicate for the present system the steady-state population in the cold trap over a rather large range of temperatures up to 100 K. It allows us to numerically control the equilibrium population expected for the rotational levels of the ions in the crystal as the perceived translational temperature is increased. The inset in the figure clearly shows how, up to about 10 K, the only levels involved would be $j = 0$ and $j = 1$, with a very small presence of $j = 2$ populations. The rather small energy spacings between the MgH^+ rotational levels, for which the first four levels span about 75 cm^{-1}, indicate also that, as the temperature increases, many more rotational levels will be occupied at the equilibrium trap temperatures indicated in Fig. 7. How fast such a collisional thermalization would occur is shown by the results presented below.

The calculations reported in Fig. 8 indicate the time evolution of the collisionally driven molecular ion populations for different values of the trap's temperature and for a fixed density of the buffer gas of $n_{\mathrm{He}} = 10^{10}$ cm^{-3}. All the temperatures reported correspond to those experimentally assessed in the Coulomb crystals in Ref. [18], while the density of the He gas is also the one indicated in the experiments.

The six panels in Fig. 8 report the six effective temperatures perceived by the localized ions that are reported in the experimental data [18]. We show the time evolution for the relative populations of the lower five ions' rotational levels, although the experimental data analyzed the behavior of only the first four rotational states as having any significant population during the cooling process.

The data indicate that the change in the perceived trap temperature is indeed a significant parameter for changing the

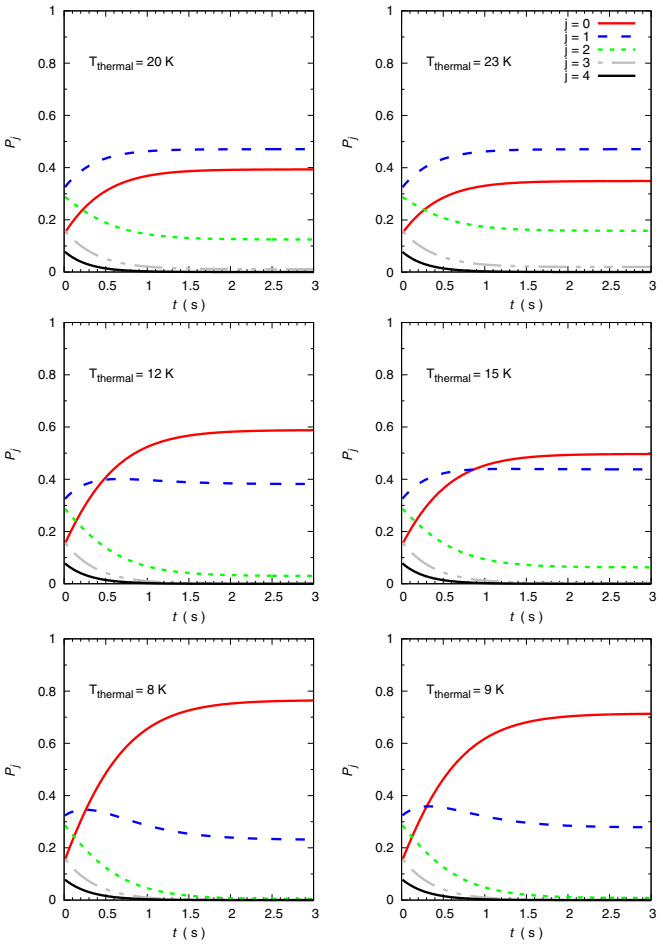

FIG. 8. Computed values of the time evolution of the MgH^+ ion's rotational-state populations by collisional perturbations in the Coulomb crystals induced by tuning the micromotion amplitudes after uploading He as a buffer gas. Temperatures are the same as those sampled in the experiments in Ref. [18] and the gas density is also the same as in the experiments: 10^{10} cm^{-3}.

relative rates of level populations during collisional rotational de-excitation processes. As T increases, in fact, we see that the two dominant population fractions are those associated with $j = 0$ and $j = 1$ states. Their relative importance, however, changes dramatically when moving from the 8–9 K region, where at the equilibrium time the $j = 0$ population is about twice that of the $j = 1$ state, to the 20–23 K region, where the two levels now have inverted populations and the $j = 1$ state is more abundant than the $j = 0$ state. This result is remarkably close to the experimental findings [18], which suggested that the rotational populations of the ion levels very quickly become those given by the thermal distributions within the trap, at the average translational temperature generated by changes in the micromotion amplitude after the uploading of the buffer gas, whose temperature remains fixed at around 8.7 K [18]. We see, in fact, from the data of the calculations shown in Fig. 8, that after at most about 3 s the relative populations have reached their steady-state values reported by the test calculations in Fig. 7. In other words, the efficient collisional energy transfer processes between MgH^+ and He, caused by changing their relative translational average energy

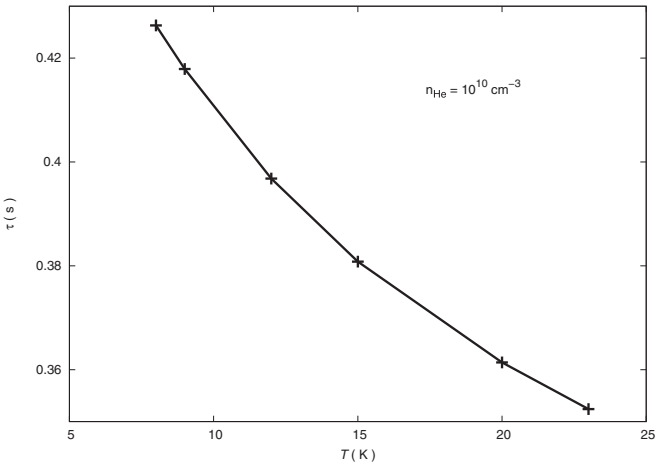

FIG. 9. Computed characteristic relaxation time τ, as defined in Eq. (9), for different translational (thermal) temperatures and for the buffer gas density value considered in the experiments.

in the trap through tuning of the micromotion amplitudes, rapidly allow the internal rotational populations of the cation to thermalize at the experimentally achieved translational temperatures in the Coulomb trap. The experimental data indeed suggest also (see Fig. 3 in Ref. [18]) that, over a fairly broad range of temperatures, the rotational temperatures are the same as the translational temperatures after the He buffer gas is uploaded to the trap. It therefore is reasonable to expect, as found in the experiments, that, after the passing of a very short time interval, ions localized within the CC environment will have reached the same temperatures for their rotational and translational degrees of freedom, as we further illustrate below.

Another useful indicator which could be extracted from the present calculations is the definition of a characteristic time, τ, which can be defined as

$$\langle E_{\rm rot}\rangle(\tau) - \langle E_{\rm rot}\rangle(t=\infty) = \frac{1}{e}(\langle (E_{\rm rot}\rangle(t=0) - \langle E_{\rm rot}\rangle(t=\infty)); \quad (9)$$

the quantity $\langle E_{\rm rot}\rangle$ represents the level-averaged rotational internal energy of the molecule in the trap after a characteristic time interval τ defined by Eq. (9). It obviously depends on the physical collision frequency and therefore it depends on the $n_{\rm He}$ value present in the trap.

The model calculations in Fig. 9 report the behavior of τ for the experimental value of the He density in the trap and for the expected range of effective thermal temperatures tested in the experiments [18]. From the data reported in that figure, we see that τ is a slow function of T, while it depends markedly on the chosen $n_{\rm He}$ value and is inversely proportional to it. The buffer gas density is the one estimated in the experiments [18] and the range of temperatures covers the values given by the experimental data in Fig. 1 in [18]. One clearly sees there that the characteristic relaxation time, i.e., the average elapsed time required to reach the rotational-to-translational temperatures, is well below 1 s, being around 0.50 s at the lower T values and only decreasing to 0.30 s at the highest experimental thermal temperatures. Such values are once

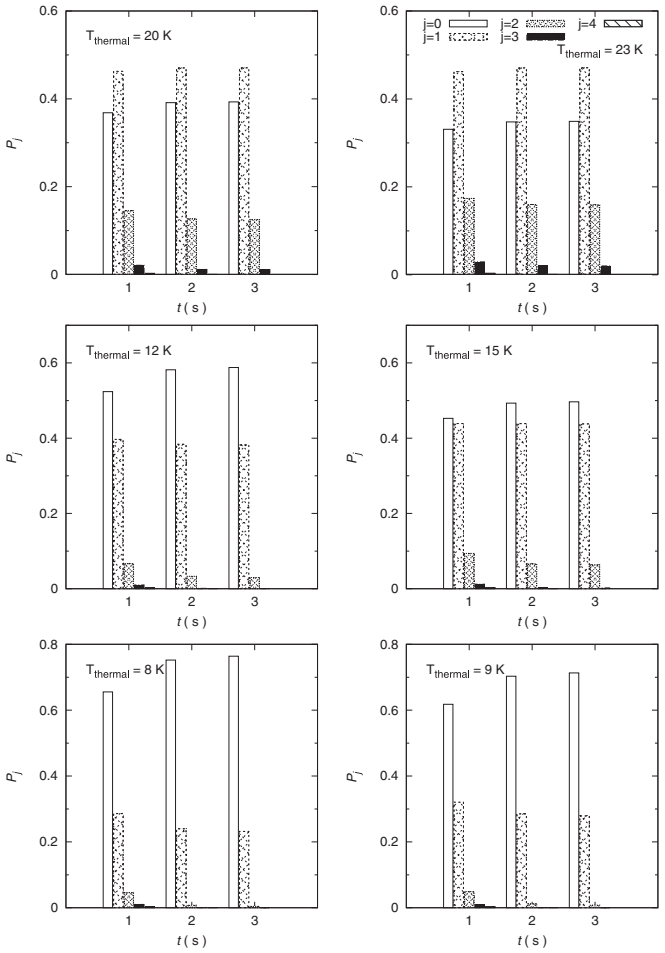

FIG. 10. Computed relative populations of the MgH^+ rotational levels in the trap, as a function of the trap's thermal temperatures and for three values(in s) of the time delay after buffer gas uploading and the ion's micromotion tuning in the experiments.

more indicative of the collisional efficiency of the rotational cooling processes for MgH^+, since similar calculations for the $OH^+(^2\Sigma)$ cation [29] indicated a τ value which was a factor of 2 larger over the same range of temperatures.

To further make contact with the experimental findings, and link our present results with the τ indicator in Fig. 9, we report in Fig. 10 the relative populations of the ion's rotational levels in the trap, as a function of the different temperatures sampled by the experiments and for different delay times after the uploading of the buffer gas in the trap and the start of the micromotion scaling to change the effective, relative translational energies within the trap. The time values shown correspond to 1, 2, and 3 s of delay after buffer gas loading.

The following considerations could be made by looking at the results shown in that figure:

(1) All panels in the figure indicate that, after 3 s at the most, the population of rotational states has reached Boltzmann's thermal distribution for each of the examined temperatures. This can be confirmed by the time evolutions in Fig. 8 and the Boltzmann's distributions in Fig. 7. This means that the rotational temperature of the molecular ions is at thermal equilibrium with its velocity distributions.

(2) With the exclusion of the two lowest temperatures, 8 and 9 K, at all other temperatures the relative populations change negligibly after the time delay is increased from 1 to 3 s. In practice, the calculations indicate that after about 1 s the rotational populations have reached their steady-state value at that temperature in each panel, while only at the lowest T values is the equilibration of the relative populations reached after a slightly longer time (see also the lowest two panels in Fig. 8).

One can therefore argue that the present collision-driven rotational population evolution in the Coulomb traps indicates a very rapid thermalization process and a very efficient energy redistribution within the MgH^+ rotational levels in order to bring the rotational temperature of the trapped ion in line with the translational temperature. The latter is the one achieved by the same CC ions after micromotion tuning of the relative collision energies following the uploading of He as the buffer gas. Thus, the ions change their relative velocities with respect to the He gas atoms but rapidly attain rotational stabilization at equilibrium with their final thermal energy. To make the comparison with the experimental findings even more transparent, we further report in Fig. 11 the relative distributions of rotational-state populations found at the five temperatures considered in the experiments (Fig. 1 in Ref. [18]) and compare them with the same distributions found by us after a time delay of 3 s in the evolution of the kinetics equations. After what has been discussed above, one should also note the rapid thermalization of the molecular rotational temperatures to the ion translational temperatures found in our calculations, a feature which confirms the experimental findings reported in Fig. 1 in Ref. [18] and shown in the right-hand panels in Fig. 11.

One can make the following considerations from a perusal of the data presented in that figure:

(1) The experimental distributions at the various rotational temperatures we consider here are very close to those obtained by solving the present master equations and extracting from the latter the distributions after an uploading time of between 1 and 3 s.

(2) The calculations suggest a very rapid, collision-driven thermalization between the internal rotational degrees of freedom of the trapped MgH^+ cation and the translational temperature experimentally generated in the trap after uploading of the buffer gas and the micromotion tuning effects. This result is in line with what has been suggested by the experimental data reported in [18].

(3) We also see from the experimental data reported in Fig. 11 that the best-fit thermal distributions given by the lighter "sticks" are very close to the rotational temperatures reported in the same panels. This is in keeping with our present findings, since we have shown that the computed rotational distributions on the right-hand side of the figure were obtained after thermalization of the ion's rotational temperatures to its steady-state translational temperatures.

(4) The experimental estimates of the refilling rates for the depleted rotational levels in the trap which are given in Ref. [18] indicate a time of about 1 s^{-1}, from which they extrapolate a rate of about 10 s^{-1} for a gas density $n_{He} = 10^{10}$ cm^{-3}. This means that the driving depletion rates, over the range of T spanned by the experiments, would be

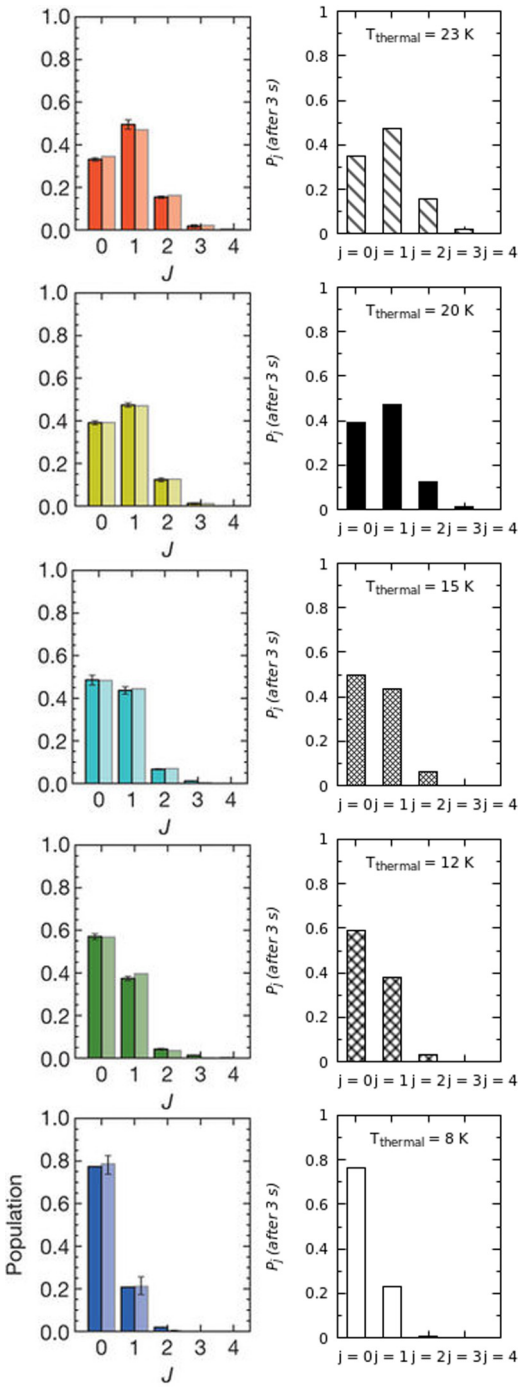

FIG. 11. Observed relative populations of the rotational states, and observed thermal distributions of the same (given by the lighter 'sticks'), for the trapped MgH^+ cation in the Coulomb crystal after uploading of the He buffer gas (panels in the left column; reproduced with permission from Ref. [18]). We also report for comparison the calculated rotational population distributions after solution of the master equation, (8), and after a time evolution delay of 3 s (panels in the right column). See the text for further details.

around 10×10^{-10} cm^3 s^{-1}. If we look at the individual state to state depletion rates computed in the present study (see Fig. 6), we see that our dominant rates for depleting the first three rotational states of MgH^+ around 10–20 K sum up to about 6.5×10^{-10} cm^3 s^{-1}. This is in good accord with the above value, especially if we note that the Langevin rate value employed in the experimental work is higher than the state-to-state cooling rates generated by the present calculations. Thus, we expect that the rate value extracted from the refilling frequencies should be lower when our computed rates are employed. Either way, however, the computed and experimentally estimated values are close to each other.

(5) One should further note that our calculated estimates of the characteristic cooling time τ in Fig. 9 are around 0.4 s at the temperature of 15 K. This corresponds to a "refilling" rate after rotational depletion of about 2 s^{-1}, which is also in line with the computed rates from the present, realistic calculations with respect to the higher Langevin rate employed in the experiments.

In conclusion, the present modeling of the collision-driven rotational cooling kinetics of MgH^+ ions trapped in a Coulomb crystal, and further exposed to the interaction with the uploaded He buffer gas, indicates this process to be rather efficient and to be within a characteristic time below 1 s. The internal rotational-state populations are shown to reach thermalization at the translational temperatures of the buffer gas under the different trap conditions which are induced by the experimental tuning of the micromotion amplitudes. This is in near quantitative agreement with the experimental findings in Ref. [18] and agrees with all the cooling dynamics features discussed for the experiments.

VI. PRESENT CONCLUSIONS

The study reported in this paper deals with the detailed computational modeling of the internal rotational-state-changing kinetics of a molecular ion, $MgH^+(^1\Sigma)$, which, experimentally, first undergoes sympathetic cooling in a Coulomb-crystal trap arrangement and then is further internally cooled by collisions with an uploaded buffer gas of He atoms. By the tuning of its micromotion amplitudes that simulate the changing of its average relative collisional energy within the trap the experiments were able to further probe different relative temperature situations between the partner ion and the uploaded gas. In order to carry out a complete computational simulation from first principles, and using a quantum *ab initio* description of the various steps involved, we have first obtained the electronic potential energy surface for the interaction between MgH^+ and He atoms. To this aim, we have employed the set of *ab initio* points reported in our earlier work [19,20] and have implemented them by generating additional points for the short-range regions of the repulsive part of the PES, as discussed and described in Sec. II. The ensuing interaction potential has been used to calculate the partial, integral, state-to-state inelastic cross sections between the lower five rotational states of the molecular ion, although only four of them have been found to be significantly populated in the experiments. From the set of inelastic cross sections, which involve excitation and de-excitation transitions between the rotational states, we have obtained the corresponding inelastic rates for the rotational "cooling" and the rotational "heating" collision-driven dynamics over a range of temperatures up to about 50 K, which is well above the experimentally tested

trap temperatures in Ref. [18] and also well above our earlier calculations for this same system [19,20].

The solution of the master equations for the time evolution of the level populations during the uploading of the buffer gas allowed us to obtain quantitative estimates of the time interval needed to deplete the rotational states of the ion in order to thermalize its rotational-state populations to the translational temperature of the trap after gas uploading. Our present results are in close agreement with the experimental findings and suggest the following:

(1) After about 1 s the internal energy distributions of the trapped ion have reached the translational temperature perceived after uploading of the buffer gas and achieved by tuning of the micromotion amplitude around a fixed He temperature of about 8.7 K. Our estimated "refilling" rate is of the order of about 1–2 s^{-1}, a value which is close to the experimental estimates of about 1 s^{-1} [18].

(2) The experimental estimate of a global cooling rate in the traps is around 10×10^{-10} $cm^3\,s^{-1}$, in line with our dominant cooling rates at around 20 K of about 6.6×10^{-10} $cm^3\,s^{-1}$.

(3) All the experimentally observed distributions between rotational states of the ion at different temperatures are in near quantitative agreement with our thermalized rotational distributions after time intervals of between 1 and 3 s.

(4) The experimentally observed equalization between rotational and thermal temperatures of the ions in the trap are confirmed by our calculations, which report the rotational distributions at the various temperatures to be very close to the thermal distributions achieved after rapidly reaching steady-state conditions in the traps.

The calculations have therefore shown very good agreement with the experimental data and suggest that the collision-driven state-changing rates for the present cations are indeed very high and indicate a very rapid process of thermalization of the rotational levels' "temperature" to the translational temperature achieved in the Coulomb-crystal environment after uploading of the He buffer gas and subsequent tuning of the ion micromotion.

ACKNOWLEDGMENTS

We thank I. Iskandarov and Lorenzo Petralia for their generous initial help in setting up the multipolar coefficients from the computed interaction potential discussed in Sec. II. L.G.S. acknowledges financial support from MINECO (Spain), Grant No. CTQ2015-65033-P. F.A.G. and R.W. thank the Austrian Science Fund (FWF), Project No. 29558-N36, for support. The computational results were obtained using in-house computer codes running on the HPC infrastructure LEO of the University of Innsbruck. This work was supported by an STSM Grant from COST Action CM1401, held by L. González-Sánchez.

[1] W. D. Phillips, Nobel lecture: Laser cooling and trapping of neutral atoms, Rev. Mod. Phys. **70**, 721 (1998).

[2] For example, see R. Krems, B. Friedrich, and W. C. Stwalley, *Cold Molecules: Theory, Experiment, Applications* (CRC Press, Boca Raton, FL, 2009).

[3] S. Willitsch, Coulomb-crystallised molecular ions in traps: Methods, applications, prospects, Int. Rev. Phys. Chem. **31**, 175 (2012).

[4] L. D. Carr, D. DeMille, R. V. Krems, and J. Ye, Cold and ultracold molecules: Science, technology and applications, New J. Phys. **11**, 055049 (2009).

[5] S. Schiller and V. Korobov, Tests of time independence of the electron and nuclear masses with ultracold molecules, Phys. Rev. A **71**, 032505 (2005).

[6] D. DeMille, Quantum Computation with Trapped Polar Molecules, Phys. Rev. Lett. **88**, 067901 (2002).

[7] M. Shapiro and P. Brumer, *Cold Molecules: Theory, Experiment, Applications* (Wiley, New York, 2003).

[8] R. V. Krems, Cold controlled chemistry, Phys. Chem. Chem. Phys. **10**, 4079 (2008).

[9] D. Hauser, S. Lee, F. Carelli, S. Spieler, O. Lakhmanskaya, E. S. Endres, S. S. Kumar, F. Gianturco, and R. Wester, Rotational state–changing cold collisions of hydroxyl ions with helium, Nat. Phys. **11**, 467 (2015).

[10] M. Viteau, A. Chotia, M. Allegrini, N. Bouloufa, O. Dulieu, D. Comparat, and P. Pillet, Optical pumping and vibrational cooling of molecules, Science **321**, 232 (2008).

[11] J. D. Weinstein, R. de Carvalho, T. Guillet, B. Friedrich, and J. M. Doyle, Magnetic trapping of calcium monohydride molecules at millikelvin temperatures, Nature **395**, 148 (1998).

[12] H. L. Bethlem, G. Berden, F. M. H. Crompvoets, R. T. Jongma, A. J. A. van Roij, and G. Meijer, Electrostatic trapping of ammonia molecules, Nature **406**, 491 (2000).

[13] T. Rieger, T. Junglen, S. A. Rangwala, P. W. H. Pinkse, and G. Rempe, Continuous Loading of an Electrostatic Trap for Polar Molecules, Phys. Rev. Lett. **95**, 173002 (2005).

[14] R. Fulton, A. I. Bishop, and P. F. Barker, Optical Stark Decelerator for Molecules, Phys. Rev. Lett. **93**, 243004 (2004).

[15] K. Mølhave and M. Drewsen, Formation of translationally cold MgH^+ and MgD^+ molecules in an ion trap, Phys. Rev. A **62**, 011401 (2000).

[16] S. Trippel, J. Mikosch, R. Berhane, R. Otto, M. Weidemüller, and R. Wester, Photodetachment of Cold OH^- in a Multipole Ion Trap, Phys. Rev. Lett. **97**, 193003 (2006).

[17] P. F. Staanum, K. Højbjerre, P. S. Skyt, A. K. Hansen, and M. Drewsen, Rotational laser cooling of vibrationally and translationally cold molecular ions, Nat. Phys. **6**, 271 (2010).

[18] A. K. Hansen, O. O. Versolato, L. Klosowski, S. B. Kristensen, A. Gingell, M. Schwarz, A. Windberger, J. Ullrich, J. R. Crespo López-Urrutia, and M. Drewsen, Efficient rotational cooling of coulomb-crystallized molecular ions by a helium buffer gas, Nature **508**, 76 (2014).

[19] M. Tacconi, F. A. Gianturco, E. Yurtsever, and D. Caruso, Cooling and quenching of $^{24}MgH^+(X^1\Sigma^+)$ by $^4He(^1S)$ in a

Coulomb trap: A quantum study of the dynamics, Phys. Rev. A **84**, 013412 (2011).

[20] D. Caruso, M. Tacconi, F. A. Gianturco, and E. Yurtsever, Quenching vibrations by collisions in cold traps: A quantum study for $MgH^+(X^1\Sigma^+)$ with $4He(^1S)$, J. Chem. Sci. **124**, 93 (2012).

[21] M. J. Frisch, G. W. Trucks, H. B. Schlegel, G. E. Scuseria, M. A. Robb, J. R. Cheeseman, J. A. Montgomery, Jr., T. Vreven, K. N. Kudin, J. C. Burant, J. M. Millam, S. S. Iyengar, J. Tomasi, V. Barone, B. Mennucci, M. Cossi, G. Scalmani, N. Rega, G. A. Petersson, H. Nakatsuji, M. Hada, M. Ehara, K. Toyota, R. Fukuda, J. Hasegawa, M. Ishida, T. Nakajima, Y. Honda, O. Kitao, H. Nakai, M. Klene, X. Li, J. E. Knox, H. P. Hratchian, J. B. Cross, V. Bakken, C. Adamo, J. Jaramillo, R. Gomperts, R. E. Stratmann, O. Yazyev, A. J. Austin, R. Cammi, C. Pomelli, J. W. Ochterski, P. Y. Ayala, K. Morokuma, G. A. Voth, P. Salvador, J. J. Dannenberg, V. G. Zakrzewski, S. Dapprich, A. D. Daniels, M. C. Strain, O. Farkas, D. K. Malick, A. D. Rabuck, K. Raghavachari, J. B. Foresman, J. V. Ortiz, Q. Cui, A. G. Baboul, S. Clifford, J. Cioslowski, B. B. Stefanov, G. Liu, A. Liashenko, P. Piskorz, I. Komaromi, R. L. Martin, D. J. Fox, T. Keith, M. A. Al-Laham, C. Y. Peng, A. Nanayakkara, M. Challacombe, P. M. W. Gill, B. Johnson, W. Chen, M. W. Wong, C. Gonzalez, and J. A. Pople, *Gaussian 03*, Revision C.02 (Gaussian, Inc., Wallingford, CT, 2004).

[22] A. Stone, *The Theory of Intermolecular Forces* (Oxford University Press, Oxford, UK, 2013).

[23] For example, see J. R. Taylor, *Scattering Theory: The Quantum Theory of Nonrelativistic Collisions. Dover Books on Engineering* (Dover, Mineola, NY, 2012).

[24] R. Martinazzo, E. Bodo, and F. A. Gianturco, A modified variable-phase algorithm for multichannel scattering with long-range potentials, Comput. Phys. Commun. **151**, 187 (2003).

[25] D. López-Durán, E. Bodo, and F. A. Gianturco, ASPIN: An all spin scattering code for atom-molecule rovibrationally inelastic cross sections, Comput. Phys. Commun. **179**, 821 (2008).

[26] L. González-Sánchez, F. A. Gianturco, and R. Wester, State–changing processes for ions in cold traps: LiH^- molecules colliding with He as a buffer gas, Mol. Opt. Phys. **49**, 235201 (2016).

[27] M. Hernández Vera, F. A. Gianturco, R. Wester, H. da Silva, Jr., O. Dulieu, and S. Schiller, Rotationally inelastic collisions of H_2^+ ions with He buffer gas: Computing cross sections and rates, J. Chem. Phys. **146**, 124310 (2017).

[28] J. Pérez-Ríos and F. Robicheaux, Rotational relaxation of molecular ions in a buffer gas, Phys. Rev. A **94**, 032709 (2016).

[29] L. González-Sánchez, F. A. Gianturco, and R. Wester, Modeling quantum kinetics in ion traps: State-changing collisions for $OH^+(^3\Sigma^+)$ ions with He as a buffer gas, Chem. Phys. Chem. **19**, 1866 (2018).

[30] S. Schiller, I. Kortunov, M. Hernández Vera, F. Gianturco, and H. da Silva, Quantum state preparation of homonuclear molecular ions enabled via a cold buffer gas: An *ab initio* study for the H_2^+ and the D_2^+ case, Phys. Rev. A **95**, 043411 (2017).

[31] M. Hernández Vera, S. Schiller, R. Wester, and F. A. Gianturco, Rotationally inelastic cross sections, rates and cooling times for para-H_2^+, ortho-D_2^+ and HD^+ in cold helium gas, Eur. Phys. J. D **71**, 106 (2017).